Self-Organization of a Plasma due to 3D Evolution of the Weibel Instability

D.V. Romanov,[1] V.Yu. Bychenkov,[1,2] W. Rozmus,[1] C. E. Capjack,[3] and R. Fedosejevs[3]
[1]*Theoretical Physics Institute, University of Alberta, Edmonton T6G2J1, Alberta, Canada*
[2]*P. N. Lebedev Physics Institute, Russian Academy of Sciences, Moscow 119991, Russia*
[3]*Department of Electrical and Computer Engineering, University of Alberta, Edmonton T6G 2J1, Alberta, Canada*
(Received 29 May 2003; published 19 November 2004)

The nonlinear evolution of the thermal Weibel instability is studied by using three-dimensional particle-in-cell simulations. After a fast saturation due to a reduction in the temperature anisotropy, the instability evolves to a quasistationary state which includes a single mode long wavelength helical magnetic field and a finite degree of temperature anisotropy. The nonlinear stability of this state is explained by periodic variations of the temperature anisotropy axis. At long time scales the magnetic field, wave number, and temperature anisotropy slowly evolve to the decreasing magnitudes.

DOI: 10.1103/PhysRevLett.93.215004 PACS numbers: 52.35.–g, 52.50.Jm, 52.59.–f, 52.65.Rr

The Weibel instability [1–3] occurs in many different plasma systems including fusion plasmas, both magnetic and inertial confinement, space plasmas, and in a new class of engineered plasmas which will soon be created by high intensity free electron x-ray laser pulses. The Weibel instability has attracted a lot of interest because it can generate a quasistationary magnetic field in a plasma [4–8]. The Weibel instability can be driven by electromagnetic radiation, electron beams, or temperature anisotropy. Numerous studies of Weibel instability have been recently conducted in short pulse laser produced plasmas (cf. Refs. [9,10] and references therein) and in the astrophysical plasmas (cf., e.g., [11]). The Weibel instability also plays an important role in the isotropization of electron temperature in plasmas created by tunnel ionization with short CO_2 laser pulses [12]. Similarly, photoionization of gaseous targets by coherent x-ray pulses, as is planned on the Tesla Test Facility [13], will allow the engineering of plasma ionization, density, and the initial parallel and transverse electron temperatures for which the Weibel instability would be important.

In this Letter we present numerical and theoretical descriptions of the thermal Weibel instability [1–3] driven by an anisotropy in the electron temperature. The term *thermal* Weibel instability is used here to differentiate between the variety of beamlike distribution functions (cf. Refs. [4,8–10]) and our classical case of a temperature anisotropy (cf. Refs. [1–3,12]). Our study is based on three-dimensional (3D) particle-in-cell simulations. The physical model involves an unmagnetized background plasma with a two temperature Maxwellian electron distribution function. Rarefied plasmas often exist in such a nonequilibrium state in the laboratory or in space until collisions or an instability relax the system to a state with an isotropic electron distribution. The nonlinear evolution of the instability for an anisotropic temperature has been studied analytically in Refs. [14–18] and by using numerical simulations in Refs. [19–24]. Different models have been employed in these studies, including a fluid approach called vortex electron anisotropic hydrodynamics (VEAH) [14,25], particle-in-cell (PIC) simulations [19,20], and Vlasov simulations [22]. The two-dimensional (2D) nonlinear regime of the Weibel instability has been studied numerically in Refs. [19,24]. Here we present PIC simulations using a fully electromagnetic, relativistic, massively parallel PIC code [26] which is applied for the first time to model the 3D evolution of a thermal Weibel instability driven by an anisotropy in the electron temperature, thus extending the previous studies of Ref. [19] to a 3D geometry.

Our PIC code solves Maxwell equations by using the Yee scheme and the particle equations of motion by a relativistic modification of the Boris scheme. The chosen particle shape factor is characterized by a well compensated self-force and slow self-heating [27]. This is an important advancement in reducing numerical self-heating. Our algorithm ensures exact charge conservation. Ions are considered immobile. Initially, at $t = 0$, the electrons have a bi-Maxwellian velocity distribution function $f \propto \exp(-m_e v_x^2/2T_{\perp 0} - m_e v_y^2/2T_{\perp 0} - m_e v_z^2/2T_{\|0})$ and are uniformly redistributed over a computational box. The number of grid cells used was $64 \times 64 \times 256$ and the number of quasiparticles was 6.3×10^7. Periodic boundary conditions are used for the electrons and for the fields. Simulations have been performed on the University of Alberta parallel computer. For a typical run, the size of the simulation box is $L_x \times L_y \times L_z = 15 \times 15 \times 60(c/\omega_{pe})$, where c is the speed of light and ω_{pe} is the electron plasma frequency. Some of the control runs have L_z 4 times smaller. Initial electron temperatures are $T_{\|0} = 0.64$ keV and $T_{\perp 0} = 16$ keV. This corresponds to a temperature anisotropy $P = T_{\perp 0}/T_{\|0} - 1 = 24$.

Figure 1 shows the evolution of the space averaged magnetic field (right axis) and thermal energies (left axis). The notation $\langle ... \rangle$ is used to indicate spatial averaging. Initially the magnetic field energy grows exponentially. The growth rate $\gamma(\mathbf{k})$ in Fig. 1 is in good agreement

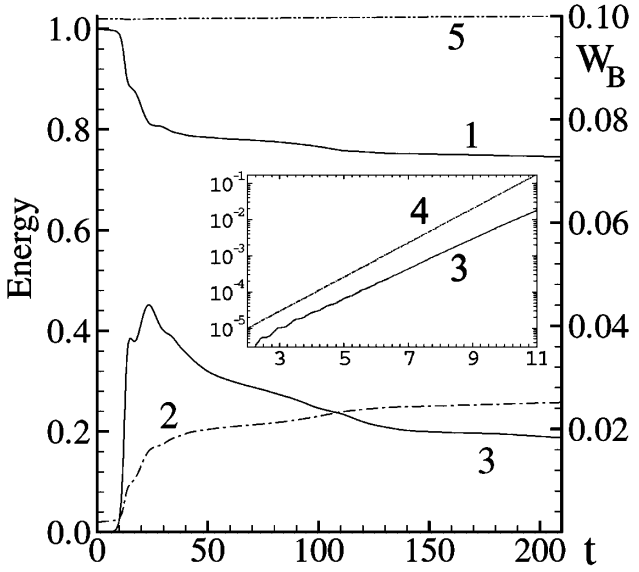

FIG. 1. Time evolution of the spatially averaged thermal energies $\langle T_\perp\rangle/T_{\perp 0}$ (1), $\langle T_\parallel\rangle/T_{\perp 0}$ (2), and magnetic field energy $W_B = \langle B^2\rangle/8\pi n T_{\perp 0}$ (3). The inset shows the initial exponential growth of the magnetic field energy (3) and analytical prediction from the linear kinetic theory (4). The total energy (5) demonstrates the accuracy of energy conservation in 3D simulation. The time unit is the plasma wave period $2\pi/\omega_{pe}$.

with the solution to the linear kinetic dispersion relation for a plasma with an anisotropic temperature (within a few percent). Along the z direction, where the growth rate reaches maximum values, $\gamma(\mathbf{k})$ can be well approximated (with an accuracy of 10% to 15%) by the expression obtained from the VEAH theory [14]:

$$\gamma(k) = k\left(\frac{T_{\parallel 0}}{m_e}\,\frac{P - c^2k^2/\omega_{pe}^2}{1 + c^2k^2/\omega_{pe}^2}\right)^{1/2}. \qquad (1)$$

The wave number domain of unstable modes is $0 < k < (\omega_{pe}/c)P$ and the characteristic wave number of the most unstable perturbation is $k \simeq 2\omega_{pe}/c$.

After experiencing exponential growth, the magnetic field saturates and the instability enters the nonlinear regime ($t \geq 20$). The nonlinear evolution comprises the transient phase ($20 \leq t \leq 130$), when the magnetic field energy is transferred to the long wavelength part of the spectrum, and the quasistationary regime ($t > 130$), which is characterized by a reduced value of the temperature anisotropy, $P \simeq 2$, a single mode magnetic field perturbation, and the slow decay of B and P. The initially small longitudinal thermal energy, $T_{\parallel 0} = 0.04T_{\perp 0}$, increases in time and saturates at $\langle T_\parallel\rangle \simeq (1/4)T_{\perp 0} \simeq (1/3)\langle T_\perp\rangle$. The high transversal temperature $T_\perp$ decreases to approximately 0.75 of its original value. The quasistationary level of the magnetic field energy is quite small, $\langle B^2/8\pi n T_{\perp 0}\rangle \approx 2 \times 10^{-2}$ (n is the electron density), which is lower than energy levels found previously in 1D and 2D simulations [19,22–24].

The first saturation of the Weibel instability is caused by the dramatic reduction in the temperature anisotropy (cf. Refs. [19,22–24]). A small fraction of the initial thermal energy is also transferred into the magnetic field perturbation. By decreasing the anisotropy one first stabilizes the growth of short wavelength perturbations. Thus in the nonlinear regime the spectrum of fluctuations is dominated by long wavelength perturbations. At late times the fluctuation spectrum peaks at the wave number corresponding to the maximum growth rate (1) for the temperature anisotropy P. For $P \simeq 2$ this approximately corresponds to $k \simeq 0.85\omega_{pe}/c$. Note that the minimum wave number ($k_{\min} = 2\pi/L_z$) which can be accommodated by the simulation box size, is $0.14\omega_{pe}/c$.

The electromagnetic energy is accumulated mainly in the magnetic field perturbations: $\langle E^2\rangle \sim (T_\perp/m_e c^2) \times \langle B^2\rangle \ll \langle B^2\rangle$. This estimate agrees well with our simulation results, where $\langle E^2\rangle/\langle B^2\rangle \lesssim 10^{-2}$. In the linear regime, a Weibel instability excites pure electromagnetic modes with $E_z = 0$, and $\delta n = 0$ where δn is the electron density perturbation. Electrostatic field and electron density perturbations develop as a nonlinear effect [14], $\delta n \sim B^2/8\pi mc^2$, reaching negligibly small levels. In practice, significantly higher density variations appear in PIC simulations due to discreteness effects. With our improved numerical algorithm we have kept the level of these numerical fluctuations below 6%.

Figure 2 shows the 3D evolution of the magnetic field: the spatial vector structure of the magnetic field is shown in the upper panels (a)–(c) and the Fourier spectrum of the magnetic field energy density is shown in the lower panels (d)–(f). For an initial temperature anisotropy, $P = 24$, modes around the twentieth spatial harmonic are the most unstable. This is in agreement with the linear theory of the Weibel instability. Because of the strong anisotropy, the instability develops over a wide cone of angles $\sim\pi/2$. The wide k spectrum at the very beginning of the Weibel instability is shown in Fig. 2(d). There are 26 unstable modes in the z direction. The initially wide cone of the unstable k vectors converges with time to a much narrower distribution with the concentration of the magnetic field energy in the z direction about the most unstable modes [Fig. 2(e)]. Finally, longer scale modes appear and the spectrum evolves to a one-mode regime featuring a helical magnetic field structure in which wave number decreases slowly in time from $k \simeq 0.8\omega_{pe}/c$ ($t = 130$) to $k \simeq 0.5\omega_{pe}/c$ ($t = 220$). The final k vector corresponds to the 4th–5th spatial harmonic for our simulation box [Fig. 2(f)]. Such an inverse cascade has been observed before in two-dimensional simulations [19].

The magnetic field evolution (Fig. 2) illustrates plasma self-organization leading to the formation of a regular helical structure from the initially chaotic plasma state. This is also shown by the k_z spectrum of the magnetic field energy in Fig. 4, which displays energy transfer

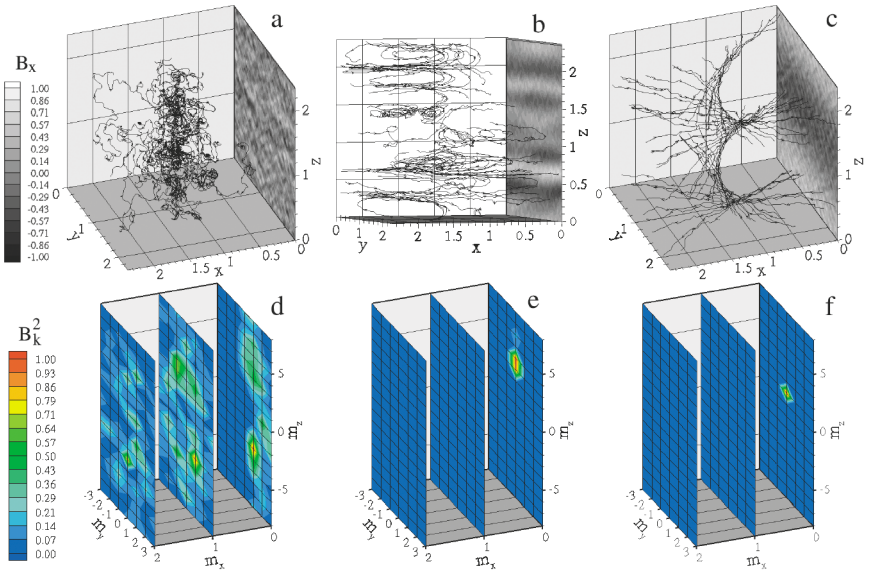

FIG. 2 (color). Spatial variations of the magnetic field and the k spectrum of magnetic field energy density ($m_i = kL_i/2\pi$, $L_i = 15c/\omega_{pe}$, $i = x, y, z$) at different time moments, $t = 3$ [(a),(d)], $t = 10$ [(b),(e)], and $t = 121$ [(c),(f)]. Magnetic field [in units of $m_e c\omega_{pe}/(2\pi e)$] and magnetic field energy spectral density are normalized to their maximum absolute values: 0.063 (a), 0.19 (b), 0.34 (c), 3.5×10^{-6} (d), 5.2×10^{-3} (e), and 0.052 (f). The top panels (a)–(c) show magnetic field lines crossing the z axis at the center of the computational box.

across the spectrum from the initial broad k-vector distribution (curve 1) to the narrow spectrum of long wavelength perturbations (curve 4) at the late time. The wave number, of the magnetic perturbations in Fig. 4, decreases as the temperature anisotropy P decreases. This is consistent with the shrinking range of linearly unstable modes as $P \to 0$. However, in the final nonlinear state corresponding to $P \approx 2$ the plasma is stable contrary to linear theory predictions. The final formation of the circularly polarized force-free magnetic field $\{B_0 \cos kz, B_0 \sin kz, 0\}$ is essentially a three-dimensional effect and therefore could not be seen in previous studies of thermal Weibel instability. Additional simulations have confirmed that our model has no bias with regard to the sign of the helicity of the final state; this depends entirely on the choice of initial conditions. The initial bi-Maxwellian electron distribution function has a pancake-like form with the anisotropy axis along the z direction (cf. Fig. 3 at $t = 0$). We define the anisotropy direction by the unit vector $\mathbf{n}$ such that the temperature tensor $\mathbf{T}$ has a diagonal form in the Cartesian reference frame defined by $\mathbf{n}$. Thus, $\mathbf{T} = T_{\|}\mathbf{nn} + T_{\perp}(\mathbf{I} - \mathbf{nn})$, where $\mathbf{n}$ points along the z direction at the initial time. The spatial and temporal evolution of the pressure anisotropy such as the rotation of the vector $\mathbf{n}$ are responsible for transition to the quasistationary nonlinear regime of the Weibel instability. At the time of first saturation of the magnetic field energy (curve three of Fig. 1 for $t \gtrsim 15$), we observe a rotation of the vector $\mathbf{n}$. This is shown in Fig. 3, where at $t = 15$, the anisotropy axis is rotated by 27° with respect to the initial direction along z axes. Such an evolution of $\mathbf{n}$ is consistent with the predictions of the reduced hydrodynamical model [28] that is derived from the VEAH equations. The analytical solution of Ref. [28] involves nonlinear periodic oscillations of the Fourier component of the magnetic field vector and the anisotropy axis $\mathbf{n}$. When the period of these oscillations is comparable with the time of linear growth, the nonlinear evolution effectively dephases and saturates the instability. The one-mode solution of Ref. [28] describes a helical magnetic field with relatively small energy, $\langle B^2 \rangle/8\pi nT_{\perp 0} \ll 1$. This is also observed in the asymptotic state of our

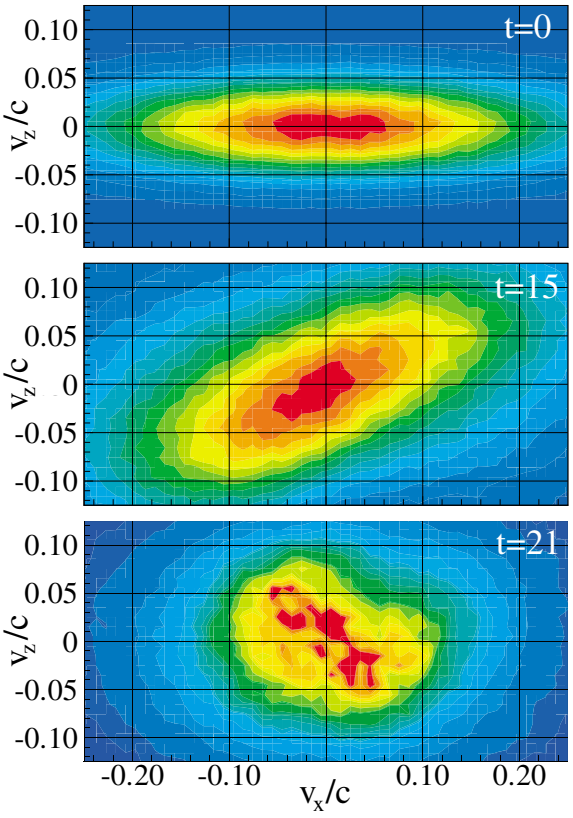

FIG. 3 (color). The electron phase space for $z \simeq 2.2c/\omega_{pe}$ at different times.

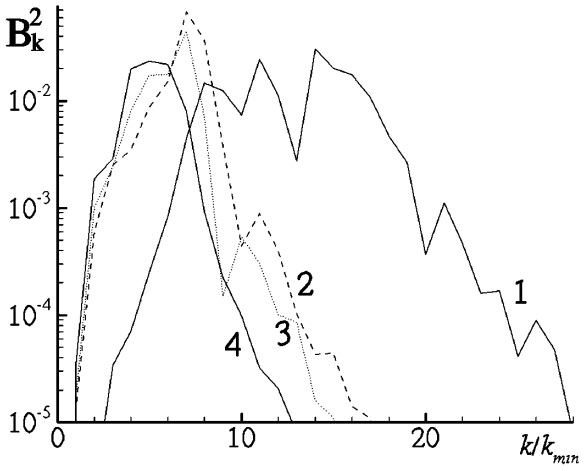

FIG. 4. Spectral density of the magnetic field energy as a function of k_z at different times: $t = 15$ (1), $t = 50$ (2), $t = 102$ (3), and $t = 210$ (4) ($k_{\min} = 2\pi\omega_{pe}/60c$).

simulations. The reduced model solution [28] and the full kinetic simulations produce similar scaling of the magnetic field amplitude $B \propto k\sqrt{P_\perp - P_\parallel}$. Thus the helical magnetic field structure is a kind of attractor leading to the self-organizing plasma. However, in the full 3D PIC simulations, the plasma evolves towards this asymptotic state in a manner far more complicated than the simple rotation of vector **n**. For example, at $t \gtrsim 21$ (cf. Fig. 3), the diagonalization of the pressure tensor displays three different diagonal elements, thus introducing another axis of the anisotropy. In particular, $P_\perp \rightarrow \{P_1, P_2\}$, where P_1 and P_2 are approximately 20% larger and smaller, respectively, than the averaged $P_\perp$ value. The complex rotation of particles in phase space occurs together with collisionless damping of electromagnetic perturbations [19,21] and thereby contributing to the plasma quasistationary state at $t > 130$. Clearly on such a long time scale, there are effects which are not included in our model such as the ion response and particle collisions which will also affect the evolution of Weibel instability.

In conclusion, we have performed 3D PIC simulations describing the nonlinear evolution of the thermal Weibel instability driven by an initial anisotropy in electron temperature. The initially broad spectrum of magnetic field turbulence evolves towards a quasistationary single mode helical structure. This scenario is in qualitative agreement with results of an analytical nonlinear model which is based on the VEAH equations.

The authors would like to thank Dr. R.W. Lee for valuable comments and discussions. This work was partly supported by the Natural Sciences and Engineering Research Council of Canada and the Russian Foundation for Basic Research (Grant No. 03-02-16428).

[1] E. M. Weibel, Phys. Rev. Lett. **2**, 83 (1959).
[2] G. Kalman *et al.*, Phys. Fluids **11**, 1797 (1968).
[3] N.W. Albright, Phys. Fluids **13**, 1021 (1970).
[4] K. Estabrook, Phys. Rev. Lett. **41**, 1808 (1978).
[5] D.W. Forslund and J. M. Kindel, Phys. Rev. Lett. **54**, 558 (1985).
[6] G. A. Askar'yan *et al.*, Pis'ma Zh. Eksp. Teor. Fiz. **60**, 240 (1994) [JETP Lett. **60**, 251 (1994)].
[7] S.V. Bulanov *et al.*, Phys. Rev. Lett. **76**, 3562 (1996).
[8] F. Califano, *et al.*, Phys. Rev. Lett. **84**, 3602 (2000).
[9] L. O. Silva *et al.*, Phys. Plasmas **9**, 2458 (2002).
[10] F. Califano *et al.*, Phys. Plasmas **9**, 451 (2002).
[11] R. A. Fonesca, L. O. Silva, J.W. Tonge, W. B. Mori, and J. M. Dawson, Phys. Plasmas **10**, 1979 (2003).
[12] W. P. Leemans *et al.*, Phys. Rev. Lett. **68**, 321 (1992).
[13] T. Tschentscher, Proc. SPIE Int. Soc. Opt. Eng. **4500**, 1 (2001).
[14] V. Yu. Bychenkov, V P. Silin, and V T. Tikhonchuk, Sov. J. Plasma Phys. **15**, 407 (1989); Phys. Lett. A **138**, 127 (1989); Theor. Math. Phys. **82**, 11 (1990); Sov. Phys. JETP **71**, 709 (1990).
[15] V. Yu. Bychenkov, Sov. J. Plasma Phys. **19**, 526 (1993).
[16] V. Yu. Bychenkov, V. F. Kovalev, and V.V. Pustovalov, Plasma Phys. Rep. **22**, 999 (1996); V. A. Terekhin *et al.*, *ibid.* **25**, 409 (1999).
[17] A. Yu. Romanov *et al.*, JETP **84**, 687 (1997).
[18] V. Yu. Bychenkov *et al.*, Plasma Phys. Rep. **26**, 54 (2000).
[19] R. L. Morse and C.W. Nielson, Phys. Fluids **14**, 830 (1971).
[20] J. M. Wallace and E. M. Epperlein, Phys. Fluids B **3**, 1579 (1991).
[21] R. C. Davidson *et al.*, Phys. Fluids **15**, 317 (1972).
[22] V. Yu. Bychenkov *et al.*, Sov. J. Plasma Phys. **17**, 272 (1991).
[23] V. Yu. Bychenkov *et al.*, Sov. J. Plasma Phys. **17**, 485 (1991).
[24] V. Yu. Bychenkov and V. N. Novikov, Plasma Phys. Rep. **23**, 671 (1997).
[25] B. Basu, Phys. Plasmas **9**, 5131 (2002).
[26] S.V. Bulanov *et al.*, Plasma Phys. Rep. **23**, 259 (1997); **25**, 701 (1999).
[27] V. A. Vshivkov *et al.*, J. Comp. Tech. **4**, 62 (1999).
[28] V. Yu. Bychenkov *et al.*, JETP Lett. **78**, 150 (2003).